JACS
JOURNAL OF THE AMERICAN CHEMICAL SOCIETY
Communication
pubs.acs.org/JACS

Nanoemulsion Contrast Agents with Sub-picomolar Sensitivity for Xenon NMR

Todd K. Stevens,[†,‡] R. Matthew Ramirez,[†,‡] and Alexander Pines*[,†,‡]

[†]Materials Science Division, Lawrence Berkeley National Laboratory, Berkeley, California 94720, United States
[‡]Department of Chemistry, University of California, Berkeley, California 94720, United States

Supporting Information

ABSTRACT: A new type of contrast agent for Xe NMR based on surfactant-stabilized perfluorocarbon-in-water nanoemulsions has been produced. The contrast agent uses dissolved hyperpolarized xenon gas as a non-perturbing reporting medium, as xenon freely exchanges between aqueous solution and the perfluorocarbon interior of the droplets, which are spectroscopically distinguishable and allow for chemical exchange saturation transfer (CEST) detection of the agent. Nanoemulsions with droplet diameters between 160 and 310 nm were produced and characterized using hyperpolarized ^{129}Xe combined with CEST detection. Saturation parameters were varied and data were modeled numerically to determine the xenon exchange dynamics of the system. Nanoemulsion droplets were detected at concentrations as low as 100 fM, corresponding to <1 μL of perfluorocarbon per liter of solution. The straightforward, inexpensive production of these agents will facilitate future development toward molecular imaging and chemical sensing applications.

The ability to detect the presence of specific analytes, whether *in vivo* or in heterogeneous solutions *in vitro*, is important for biomedical research[1] as well as chemical sensing platforms.[2,3] Such applications often require sensitive detection to report on small quantities of the material of interest. Nuclear magnetic resonance (NMR) is a well-established technique which can non-invasively probe opaque samples without the use of ionizing radiation. NMR most often employs protons to generate signal, but its utility for low detection applications is limited by its poor sensitivity, especially in aqueous solutions where the large water signal presents a challenge of dynamic range for detecting sparse analytes. Here, we describe a contrast agent that operates on ^{129}Xe rather than protons, is easily prepared from inexpensive materials, and can be detected at sub-picomolar concentrations.

One approach for improving the sensitivity of ^{1}H NMR for molecular and environmental sensing has been the development of indirect detection strategies utilizing chemical exchange saturation transfer (CEST).[4] CEST contrast arises from the selective saturation of a small pool of spectroscopically resolved nuclei that are in continuous exchange with a larger bulk pool of nuclei. If the saturation pulse duration is long relative to the mean residence time of the nuclei in the small pool, a buildup of saturated spins in the bulk pool will result in a readily observed signal decrease of the large bulk signal. Unlike most contrast mechanisms, CEST can be arbitrarily turned on or off. Many variations of this general technique, including the use of paramagnetic shift reagents (PARACEST) and endogenous proton exchange (DIACEST), have been successfully applied both *in vitro* and *in vivo*.[5−11]

In the present work, rather than water protons, the sensing medium consists of dissolved ^{129}Xe gas. Xenon is an ideal reporter because it is inert and nontoxic, and has no background in natural samples. Its NMR-active isotope, ^{129}Xe, is 26.4% naturally abundant, and, most importantly, can be hyperpolarized using established optical pumping techniques to generate non-thermal spin distribution resulting in large signals from small concentrations of ^{129}Xe.[12,13] Agents utilizing the complementary sensitivity enhancements of both hyperpolarized ^{129}Xe and CEST have been developed.[14,15] These "hyperCEST" agents employ cryptophane-A molecular cages to reversibly bind dissolved xenon and impart a large frequency shift to the bound ^{129}Xe nuclei,[16] and have achieved sub-picomolar detection thresholds when mutiple cages are assembled on protein scaffolds.[17,18]

The key to achieving low detection thresholds with these agents lies in the large signal-per-spin afforded by hyperpolarization, making ^{129}Xe well-suited to detecting small changes from the presence of small quantities of hyperCEST agents. Since the concentration of bulk pool xenon is often <1 mM, even modest saturation due to CEST elicits signficant contrast. For instance, a contrast of 20% represents saturation of ∼70 μM of xenon, assuming [Xe] = 350 μM, whereas the same contrast for a proton-CEST agent represents saturation of ∼20 M of water protons. A drawback to cryptophane-based hyperCEST agents, however, is the difficulty of their synthesis.[19]

In this study, a new type of ^{129}Xe hyperCEST agent based on perfluorocarbon (PFC) nanoemulsions is presented, which is easily prepared from readily available materials. In addition to their previous use as agents for ^{19}F MRI[20,21] and ultrasound,[21] PFC nanoemulsions have been used as vehicles for localized drug delivery.[22] At the core of these nanoemulsions (Figure 1a,b) is a short, linear PFC, perfluorooctyl bromide (PFOB), which has excellent Xe gas solubility (Xe Ostwald solubility coefficient ∼1.2 at 37 °C, about 10 times higher than Xe solubility in water).[23] Such nanoemulsions have been used previously as blood substitutes because of their ability to

Received: March 22, 2013
Published: June 7, 2013

   dx.doi.org/10.1021/ja402885q | J. Am. Chem. Soc. 2013, 135, 9576−9579

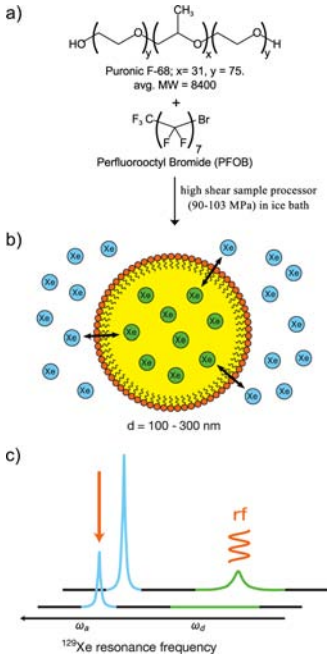

Figure 1. Preparation and hyperCEST detection of surfactant-stabilized PFOB nanoemulsions. (a) Nanoemulsion droplets were prepared by passing an aqueous solution containing a nonionic surfactant, F-68, and perflourooctyl bromide (PFOB) through a high shear sample processor. Xenon atoms exchange between the PFOB interior of the droplets and the bulk aqueous pool (b), leading to two unique peaks in the ^{129}Xe spectrum (c). Indirect detection of these agents is performed by frequency-selective rf saturation at the chemical shift of ^{129}Xe in droplets, ω_d, and exchange transfers saturated spins to the bulk aqueous ^{129}Xe pool, reducing its signal at ω_a.

solubilize oxygen.[24] Importantly, ^{129}Xe dissolved in PFOB has a unique chemical shift ($\omega_p \approx 100$ ppm, referenced to the ^{129}Xe gas signal) that is well-separated from ^{129}Xe dissolved in aqueous solutions ($\omega_a \approx 192$ ppm), and has long T_1 relaxation times in this medium.[23] Furthermore, xenon has been shown to exchange in and out of larger emulsified droplets that have been proposed as carrier agents for intravenous hyperpolarized ^{129}Xe injection.[23,25] On the basis of these characteristics, it was hypothesized that PFOB nanoemulsion droplets could be detected with a hyperCEST scheme (Figure 1c) that would benefit from both a large number of xenon atoms dissolved within each droplet and more rapid xenon exchange dynamics compared to those of cryptophane hosts, producing more contrast per agent. This is an analogous approach to the development of proton-based LIPOCEST agents by Aime and colleagues, where supramolecular vesicles doped with paramagnetic shift reagents were used to tune and harness of the exchange of a large number of encapsulated water molecules to maxmize per-agent PARACEST contrast.[8,9,26]

Nanoemulsions were produced with a high shear sample processor (M-110S Microfluidizer, Microfluidics Corp., Newton, MA) yielding nanoemulsions with narrow droplet size distributions (polydispersity indices <0.1). The poloxamer surfactant (Pluronic F-68, average MW = 8400, BASF, USA) proved effective at stabilizing the droplets as evidenced by the low polydispersities and slow growth curves as seen by dynamic light scattering (DLS). Droplets were ∼130 nm one hour after processing, and their slow growth followed a power function (Supporting Information, SI). Slow droplet growth coupled with consistently small size polydisperisty allowed for the successive selection over time of nanoemulsions with increasing average droplet diameters (160, 210, 265, and 310 nm), which were subsequently used at varying dilutions. Table 1 outlines the relevant properties of the nanoemulsion droplets used in this study.

Table 1. Nanoemulsion Droplet Characteristics

$d_{droplet}$ (nm)	$V_{droplet}$ ($\times 10^{-18}$ L)	$N_{Xe,droplet}$ ($\times 10^{5}$)[a]	τ_d (μs)[b]	[droplet] ($\times 10^{-12}$ mol/L)	relative total droplet volume (μL/L)
160	1.77	6.6	27	231	246
210	4.19	14.9	48	93	235
265	8.18	30.0	76	43	212
310	14.14	48.0	104	26	221

[a]Calculated from the xenon Ostwald solubility for PFOB: $[Xe_{aq}] = 5.1$ M.[23] [b]Determined from the McConnell–Bloch model of the data (see SI).

Hyperpolarized ^{129}Xe gas was prepared from a pressurized xenon gas mixture (2% natural abundance xenon, 10% nitrogen, 88% helium at 550 kPa) by spin-exchange optical pumping with a MITI XenoSpin polarizer (P ≈ 5%; GE Healthcare, formerly Nycomed Amersham). All NMR was performed at 7.05 T on a Varian ^{UNITY}INOVA vertical bore spectrometer with a commercial, dual-tuned (^{1}H/^{129}Xe) 5-mm probe and the temperature regulated at 37 °C. Full CEST spectra displayed high signal-to-noise ratio (SNR) and no baseline distortion (Figure 2a). Similarly consistent data quality was achieved for the saturation time experiments as evidenced by the small error bars for each time point seen in Figure 2c,d. The stability of the ^{129}Xe signal (so-called "shot noise") is particularly important since signal changes are calculated from two independent acquisitions. In these experiments, the relative standard deviation was 3%.

CEST spectra for increasing droplet sizes (Figure 2a) demonstrated the slowing of the effective xenon exchange rate due to the diffusion-limited xenon residence times in the droplets. A similar effect has been reported for LIPOCEST agents, although the exchange rates observed in that case were in the slow exchange regime, and thus particles with smaller droplet sizes (faster exchange rates) were more efficient CEST agents.[27] Here, the opposite trend was observed. The series of spectra in Figure 2 capture the transition from fast-intermediate chemical exchange in the 160 nm droplets, as evidenced by a single asymmetric saturation resonance (Figure 2a, yellow), to slow-intermediate chemical exchange for the largest droplet sizes, as evidenced by two clearly delineated saturation resonances (Figure 2a, blue, green). The agent concentrations were adjusted so that the total PFOB volume fraction was constant between the samples, thereby isolating the effect of the xenon exchange rate on saturation transfer. The total particle volume was ∼230 μL per liter of solution.

The effect of changing saturation time was also measured for two series of droplet dilutions. The 210 nm droplets were detectable at concentrations as low as 1 pM (2.52 μL particle per liter of solution; Figure 2c), while the 310 nm droplets were detectable as low as 100 fM (0.85 μL particle per liter of solution; Figure 2d) using saturation powers that appear generally compatible with *in vivo* specific absorption rate (SAR) constraints. (Note: due to the low gyromagnetic ratio of ^{129}Xe, 51 μT continuous wave (cw) irradiation for ^{129}Xe is the SAR equivalent of a 14 μT cw pulse applied at ^{1}H carrier

dx.doi.org/10.1021/ja402885q | J. Am. Chem. Soc. 2013, 135, 9576–9579

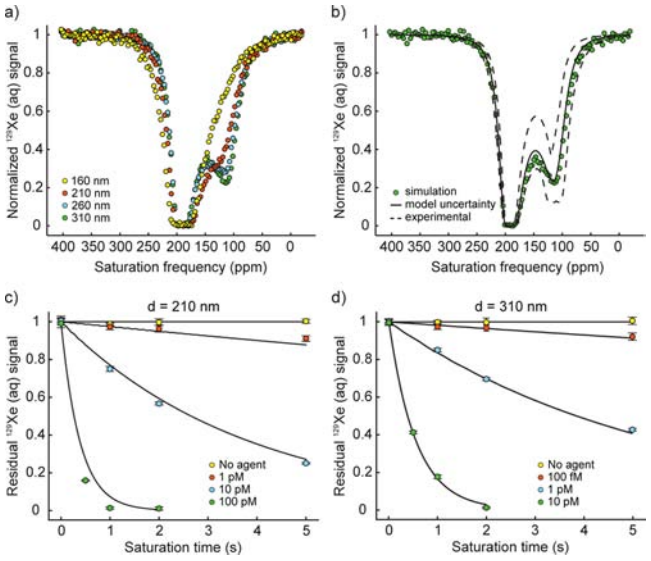

Figure 2. ^{129}Xe hyperCEST response changes with droplet size. (a) CEST spectra for 160, 210, 265, and 310 nm diameter nanoemulsion droplets at 37 °C. Shown in each plot is the aqueous ^{129}Xe signal after a 2 s, 21 μT cw saturation applied at varying offset frequencies. Concentrations were adjusted so that the droplet volume fraction was constant for all samples (~230 μL agent per liter of solution). (b) Representative plot showing results of simultaneously fitting all experimental data to the McConnell–Bloch model. The model best fit (solid line) matches well to experimental data (circles). Also shown is the confidence interval of the model based on the standard deviations of the fitted parameters (dotted lines). (c,d) Residual aqueous ^{129}Xe signal (1 − Contrast, equal to I_{on}/I_{off}) vs saturation time for a series of dilutions of 210 nm (c) and 310 nm (d) diameter droplets at 37 °C. Note: 1 pM = 2.52 μL/L (d = 210 nm) or 8.51 μL/L (310 nm). Shown for each dilution is the residual aqueous ^{129}Xe signal following rf saturation (circles) with the superimposed McConnell–Bloch model of best fit (solid line). Error bars represent standard deviation of the set of four saturation measurements.

frequencies.) All reported contrasts were generated within 5 s, a much shorter saturation duration than required to produce similar detection thresholds with other ^{129}Xe contrast agents.[17,18]

The McConnell–Bloch equations accurately characterized the xenon exchange dynamics of the system as seen by the agreement between the fit model and the data (Figure 2b–d). The model accommodated concurrent variations in the important experimental CEST parameters—namely the droplet size, total PFOB volume, and the saturation power and duration. The xenon escape probability was determined to be 1.4 ± 0.5%, from which the droplet size-dependent xenon residence time τ_d was derived[23,28] to be ~$5\overline{d}^2/D$ (see SI). The ^{129}Xe chemical shift in the PFOB droplets was determined to be 111 ± 9 ppm. The inclusion of droplet size distributions representing the sample polydispersities produced only minimal improvements in the fit, but not beyond what was expected for the increased degree of freedom of the model function. Similarly, when allowing the escape probability to vary proportionally with an arbitrary exponential of the droplet size, no significant improvements in the fit of the data were realized.

The sensitivity of these PFC nanoemulsions is competitive with iron oxide particles, which have been detected as single, micrometer-sized particles in 100^3 μm^3 voxels (~1 μL particle per liter of solution).[29] Unlike iron oxides, however, contrast from PFC nanoemulsion agents can be switched on and off at will, and the use of ^{129}Xe as the reporting medium eliminates confounding background signals in aqueous environments. Though direct imaging of the ^{19}F signal from the fluorines of the nanoemulsion PFC core is possible by NMR and also affords the advantage of zero background, the per nucleus sensitivity is similar to that of ^{1}H NMR.[30] Noting that the fluorine concentration at the most prominent PFOB signal (CF_3) was ~9 μM in the most dilute nanoemulsion sample detected by hyperCEST (Figure 2d), the described hyperCEST scheme is capable of detecting droplet concentrations that are ~2 orders of magnitude lower than those detectable by ^{19}F detection with comparable hardware. Although the better temporal resolution of ^{19}F measurements would allow for a signal averaging advantage over hyperCEST, this benefit would be most pronounced for millimolar CF_3 fluorine concentrations or higher at which direct ^{19}F measurements are more capable at extracting signal from the noise.

In the present study, the pressurized gas mixture used for hyperpolarization (2% Xe, natural abundance; partial pressure = 0.109 atm) was routed directly from the polarizer to the phantom and bubbled through the solution. With the solution temperature controlled at 37 °C, the concentration of xenon dissolved in water was 357 μM, 26% of which was ^{129}Xe, meaning that the signal-producing concentration of xenon was just 94 μM. Signal can be increased by increasing the concentration of dissolved ^{129}Xe, for example by physically separating xenon from the polarization mixture, or by isotopic enrichment of ^{129}Xe. Implementing these together would increase signal by nearly 200 times. Furthermore, technological and engineering improvements to xenon polarizer design have resulted in instruments capable of producing ^{129}Xe polarized to 50% at rates exceeding 1 liter per hour.[31] These polarization levels are important for imaging micromolar quantities of dissolved xenon, especially in complex mixtures.

The feasibility of direct MR imaging ^{129}Xe of dissolved in lung tissue has been demonstrated,[32,33] and this nanoemulsion system could prove useful for detecting cancer in lung tissues. Similar, actively targeted nanoemulsion particles have been produced,[34] but such agents could also rely on passive targeting through the enhanced permeability and retention (EPR) effect in which small molecules tend to aggregate inside of tumor tissue as a result of abnormally large pores in the vasculature of tumors.[35] Indeed, several reports demonstrating the efficacy of PFC nanoemulsions for labeling tumors have relied upon such accumulation over time.[36,37] In addition to the issue of pathology-specific agent distribution, the most important considerations for future *in vivo* molecular imaging with the nanoemulsion hyperCEST agents will be (a) the availability of the bound agents to circulating and diffusing xenon and the time scale and dynamics of the agent–xenon interactions relative to the T_1 relaxation of the hyperpolarized bulk ^{129}Xe signal, (b) the size of targeted pathologies relative to achievable dissolved-phase lung imaging resolutions, and (c) the changes to rf sensitivity due to larger coil geometries and sample displacements.

Future work will aim to extend control over the droplet sizing and stability by altering the composition of the membrane layer which will change the xenon permeability and thus the sensitivity of these agents. The data suggest that slowing the xenon exchange rate will enhance contrast on a per agent basis. This may be achieved by incorporating different surfactants such as cross-linking phospholipids or fluorine-

dx.doi.org/10.1021/ja402885q | J. Am. Chem. Soc. 2013, 135, 9576–9579

containing block copolymers. Further refinement of these hyperCEST agents will benefit from ongoing development of the biocompatibility[36−38] and active-targeting[34] of PFC nanoemulsions as contrast agents for ^{19}F MRI and ultrasound, and as localized drug delivery carriers. Moreover, the flexibility of PFC nanoemulsions to act as contrast agents across various imaging platforms means that multimodal versions of these agents are readily accessible.[39,40]

In conclusion, a new class of hyperpolarized ^{129}Xe NMR contrast agent based on PFC nanoemulsions has been demonstrated. The presence of these agents was detected *in vitro* at sub-picomolar concentrations using a hyperCEST detection scheme. The straightforward preparation of these nanoemulsions will facilitate future development for applications such as chemical sensing or molecular imaging in systems where ^{129}Xe can be employed as a reporting NMR medium.

■ ASSOCIATED CONTENT

Ⓢ Supporting Information

Experimental procedures and data. This material is available free of charge via the Internet at http://pubs.acs.org.

■ AUTHOR INFORMATION

Corresponding Author

pines@berkeley.edu

Notes

The authors declare no competing financial interest.

■ ACKNOWLEDGMENTS

Research was supported by the U.S. Department of Energy, Office of Basic Energy Sciences, Division of Materials Sciences and Engineering under Contract No. DE-AC02-05CH11231, and by an NSERC Canada Postdoctoral Fellowship award (T.K.S.). We thank Vikram S. Bajaj for feedback when preparing the manuscript.

■ REFERENCES

(1) Massoud, T. F.; Gambhir, S. S. *Gene Dev.* **2003**, *17*, 545.
(2) Perez, J. M.; Josephson, L.; O'Loughlin, T.; Hogemann, D.; Weissleder, R. *Nat. Biotechnol.* **2002**, *20*, 816.
(3) Mogensen, K. B.; Klank, H.; Kutter, J. P. *Electrophoresis* **2004**, *25*, 3498.
(4) Ward, K. M.; Aletras, A. H.; Balaban, R. S. *J. Magn. Reson.* **2000**, *143*, 79.
(5) Zhang, S.; Merritt, M.; Woessner, D. E.; Lenkinski, R. E.; Sherry, A. D. *Acc. Chem. Res.* **2003**, *36*, 783.
(6) Zhou, J.; Lal, B.; Wilson, D. A.; Laterra, J.; van Zijl, P. *Magn. Reson. Med.* **2003**, *50*, 1120.
(7) Zhang, S.; Malloy, C. R.; Sherry, A. D. *J. Am. Chem. Soc.* **2005**, *127*, 17572.
(8) Aime, S.; Carrera, C.; Delli Castelli, D.; Geninatti Crich, S.; Terreno, E. *Angew. Chem., Int. Ed.* **2005**, *44*, 1813.
(9) Aime, S.; Castelli, D. D.; Terreno, E. *Angew. Chem., Int. Ed.* **2005**, *44*, 5513.
(10) van Zijl, P. C.; Jones, C. K.; Ren, J.; Malloy, C. R.; Sherry, A. D. *Proc. Natl. Acad. Sci. U.S.A.* **2007**, *104*, 4359.
(11) McMahon, M. T.; Gilad, A. A.; DeLiso, M. A.; Cromer Berman, S. M.; Bulte, J. W.; van Zijl, P. *Magn. Reson. Med.* **2008**, *60*, 803.
(12) Walker, T. G.; Happer, W. *Rev. Mod. Phys.* **1997**, *69*, 629.
(13) Goodson, B. M. *J. Magn. Reson.* **2002**, *155*, 157.
(14) Schröder, L.; Lowery, T. J.; Hilty, C.; Wemmer, D. E.; Pines, A. *Science* **2006**, *314*, 446.
(15) Schröder, L.; Meldrum, T.; Smith, M.; Lowery, T. J.; Wemmer, D. E.; Pines, A. *Phys. Rev. Lett.* **2008**, *100*, 257603.
(16) Spence, M. M.; Rubin, S. M.; Dimitrov, I. E.; Ruiz, E. J.; Wemmer, D. E.; Pines, A.; Yao, S. Q.; Tian, F.; Schultz, P. G. *Proc. Natl. Acad. Sci. U.S.A.* **2001**, *98*, 10654.
(17) Meldrum, T.; Seim, K. L.; Bajaj, V. S.; Palaniappan, K. K.; Wu, W.; Francis, M. B.; Wemmer, D. E.; Pines, A. *J. Am. Chem. Soc.* **2010**, *132*, 5936.
(18) Stevens, T. K.; Palaniappan, K. K.; Ramirez, R. M.; Francis, M. B.; Wemmer, D. E.; Pines, A. *Magn. Reson. Med.* **2013**, *69*, 1245.
(19) Brotin, T.; Dutasta, J. P. *Chem. Rev.* **2009**, *109*, 88.
(20) Ahrens, E. T.; Flores, R.; Xu, H.; Morel, P. A. *Nat. Biotechnol.* **2005**, *23*, 983.
(21) Díaz-López, R.; Tsapis, N.; Fattal, E. *Pharm. Res.* **2010**, *27*, 1.
(22) Sarker, D. K. *Curr. Drug Deliv.* **2005**, *2*, 297.
(23) Wolber, J.; Rowland, I. J.; Leach, M. O.; Bifone, A. *Magn. Reson. Med.* **1999**, *41*, 442.
(24) Riess, J. G. *Artif. Cell Blood Sub.* **2006**, *34*, 567.
(25) Gherase, M. R.; Wallace, J. C.; Cross, A. R.; Santyr, G. E. *J. Chem. Phys.* **2006**, *125*, 044906.
(26) Terreno, E.; Cabella, C.; Carrera, C.; Delli Castelli, D.; Mazzon, R.; Rollet, S.; Stancanello, J.; Visigalli, M.; Aime, S. *Angew. Chem.* **2007**, *119*, 984.
(27) Zhao, J. M.; Ya-el, H.-e.; McMahon, M. T.; Zhou, J.; Sherry, A. D.; Sgouros, G.; Bulte, J. W. M.; van Zijl, P. C. M. *J. Am. Chem. Soc.* **2008**, *130*, 5178.
(28) Hey, M. J.; Al-Sagheer, F. *Langmuir* **1994**, *10*, 1370.
(29) Heyn, C.; Bowen, C. V.; Rutt, B. K.; Foster, P. J. *Magn. Reson. Med.* **2005**, *53*, 312.
(30) Ruiz-Cabello, J.; Barnett, B. P.; Bottomley, P. A.; Bulte, J. W. *NMR Biomed.* **2011**, *24*, 114.
(31) Hersman, F. W.; Ruset, I. C.; Ketel, S.; Muradian, I.; Covrig, S. D.; Distelbrink, J.; Porter, W.; Watt, D.; Ketel, J.; Brackett, J. *Acad. Radiol.* **2008**, *15*, 683.
(32) Cleveland, Z. I.; Cofer, G. P.; Metz, G.; Beaver, D.; Nouls, J.; Kaushik, S. S.; Kraft, M.; Wolber, J.; Kelly, K. T.; McAdams, H. P.; Driehuys, B. *PLoS ONE* **2010**, *5*, e12192.
(33) Mugler, J. P., III; Altes, T. A.; Ruset, I. C.; Dregely, I. M.; Mata, J. F.; Miller, G. W.; Ketel, S.; Ketel, J.; Hersman, F. W.; Ruppert, K. *Proc. Natl. Acad. Sci. U.S.A.* **2010**, *107*, 21707.
(34) Kaneda, M. M.; Caruthers, S.; Lanza, G. M.; Wickline, S. A. *Ann. Biomed. Eng.* **2009**, *37*, 1922.
(35) Matsumura, Y.; Maeda, H. *Cancer Res.* **1986**, *46*, 6387.
(36) Díaz-López, R.; Tsapis, N.; Santin, M.; Bridal, S. L.; Nicolas, V.; Jaillard, D.; Libong, D.; Chaminade, P.; Marsaud, V.; Vauthier, C. *Biomaterials* **2010**, *31*, 1723.
(37) Diou, O.; Tsapis, N.; Giraudeau, C.; Valette, J.; Gueutin, C.; Bourasset, F.; Zanna, S.; Vauthier, C.; Fattal, E. *Biomaterials* **2012**, *33*, 5593.
(38) Díaz-López, R.; Tsapis, N.; Libong, D.; Chaminade, P.; Connan, C.; Chehimi, M. M.; Berti, R.; Taulier, N.; Urbach, W.; Nicolas, V.; Fattal, E. *Biomaterials* **2009**, *30*, 1462.
(39) Lim, Y. T.; Noh, Y.-W.; Kwon, J.-N.; Chung, B. H. *Chem. Commun.* **2009**, *45*, 6952.
(40) Lim, Y. T.; Noh, Y. W.; Cho, J. H.; Han, J. H.; Choi, B. S.; Kwon, J.; Hong, K. S.; Gokarna, A.; Cho, Y. H.; Chung, B. H. *J. Am. Chem. Soc.* **2009**, *131*, 17145.